

Infrared conductivity of a $d_{x^2-y^2}$ -wave superconductor with impurity and spin-fluctuation scattering

S. M. Quinlan

*Solid State Division, Oak Ridge National Laboratory, P.O. Box 2008, Oak Ridge, TN 37831-6032
and Department of Physics and Astronomy, University of Tennessee, Knoxville, TN 37996-1200*

P. J. Hirschfeld

Department of Physics, University of Florida, Gainesville, FL 32611

D. J. Scalapino

Department of Physics, University of California, Santa Barbara, CA 93106-9530

(October 16, 1995)

Abstract

Calculations are presented of the in-plane far-infrared conductivity of a $d_{x^2-y^2}$ -wave superconductor, incorporating elastic scattering due to impurities and inelastic scattering due to spin fluctuations. The impurity scattering is modeled by short-range potential scattering with arbitrary phase shift, while scattering due to spin fluctuations is calculated within a weak-coupling Hubbard model picture. The conductivity is characterized by a low-temperature residual Drude feature whose height and weight are controlled by impurity scattering, as well as a broad peak centered at $4\Delta_0$ arising from clean-limit inelastic processes. Results are in qualitative agreement with experiment despite missing spectral weight at high energies.

74.25.Nf, 74.72.-h, 72.10.Di, 72.10.Fk

Typeset using REVTeX

I. INTRODUCTION

Infrared studies of the classic low-temperature superconductors provided evidence for the existence of a superconducting energy gap as well as information on the phonon-mediated pairing interaction.^{1,2} In particular, at a low reduced temperature T/T_c , the conductivity $\sigma_1(\omega)$ of an s -wave superconductor shows an onset when ω exceeds 2Δ , increasing to the normal-state value at frequencies several times 2Δ .³ Further, structure in $\sigma_1(\omega)$ at $2\Delta + \omega_p$ reflects peaks at ω_p in the effective phonon mediated interaction $\alpha^2F(\omega)$ and a detailed measurement of $\sigma_1(\omega)$ can in principle² be used to determine $\alpha^2F(\omega)$. Thus it was hoped that infrared measurements of $\sigma_1(\omega)$ for the high-temperature superconducting cuprates would provide similar information on both the gap and the pairing mechanism. However, the search for evidence of an energy gap in the cuprates has proven difficult.⁴ In spite of a confluence of data on high-quality samples, there has been a wide, even divergent, view on the interpretation of these data.

The solid curves in Fig. 1 show experimental results for the a -axis conductivity $\sigma_1(\omega)$ of an untwinned $\text{YBa}_2\text{Cu}_3\text{O}_{6.93}$ crystal.⁵ The a -axis conductivity, which avoids the chains, is believed to provide a probe of the properties of the CuO_2 planes. In the normal state $\sigma_1(\omega)$ exhibits a much larger spectral weight at high frequencies than would be present from a Drude form with a frequency independent lifetime. Various interpretations of this have been suggested. It has been proposed⁴ that this behavior reflects a two-component response consisting of a “free-carrier” Drude piece and a mid-infrared (MIR) contribution associated with “bound-carriers.” Alternatively, a one-component quasiparticle description in which the quasiparticle scattering rate $\tau^{-1} = b \max(T, \omega)$ has also been used to fit the normal state data.⁶ However, a consistent fit with constant prefactor b cannot be obtained in frequency ranges both above and below $\sim 1000 \text{ cm}^{-1}$.⁷

Likewise, in the superconducting state, various explanations of the data have been proposed. In the two-component picture, it is argued^{4,8,9} that the “free-carriers” condense to form the superfluid while the “bound-carriers” remain, giving rise to the MIR structure

which becomes more clearly visible below T_c . In this view the mean free path of the free-electron component is large compared to ξ_0 so that one is in the clean limit in which it is difficult to see the 2Δ onset of $\sigma_1(\omega)$. Moreover, the MIR absorption acts to obscure any small onset feature. An alternative explanation¹⁰ assigned the structure beginning at 500 cm^{-1} to an s -wave 2Δ onset, giving $2\Delta_0/kT_c \sim 8$. The problem in this case is to understand the low-temperature absorption clearly visible below 2Δ .

Recently, following various experiments¹¹ which suggest that the high-temperature cuprates are characterized by a non- s -wave gap, there have been several explanations for the infrared data based on a gap with nodes. Putikka and Hirschfeld calculated the ab plane conductivity for a $d_{x^2-y^2}$ state over a cylindrical Fermi surface, including impurity scattering with arbitrary phase shift.¹² Carbotte *et al.*¹³ have reported $\sigma_1(\omega)$ calculations for a model with a gap $\Delta_0 \cos\theta$. They include impurity scattering within the Born approximation and treat the dynamics within a Migdal-Eliashberg approximation in which a Pb spectrum or alternatively a cut-off Lorentzian are used as models for the electron-boson spectral density. Basov *et al.*¹⁴ have discussed the infrared conductivity in $\text{YBa}_2\text{Cu}_3\text{O}_{6.95}$ crystals which have been ion irradiated in terms of a possible d -wave state and carrier localization produced by the ion irradiation. Sauls and co-workers have calculated both the in-plane and c -axis conductivities of a $d_{x^2-y^2}$ superconductor including impurity scattering with arbitrary phase shift but neglecting inelastic scattering.¹⁵

Here we propose to extend previous calculations of the microwave response for a $d_{x^2-y^2}$ -wave superconductor to the infrared regime. Our basic strategy is the same as in the previous work:¹⁶ we seek a minimal model consisting of a $d_{x^2-y^2}$ BCS superconductor with quasiparticles whose inverse lifetimes are given by the sum of elastic impurity scattering and inelastic spin-fluctuation scattering $1/\tau \equiv 1/\tau_{\text{in}} + 1/\tau_{\text{imp}}$. The inelastic scattering rate is calculated from a spin-fluctuation exchange interaction which depends upon the $d_{x^2-y^2}$ gap and was previously found to give a reasonable fit to the temperature-dependent quasiparticle lifetime determined by the microwave measurements.¹⁷ For the present case, the dynamic frequency dependence of the lifetime will be important. While a more complete theory is

needed, we believe that it is useful to understand to what extent this minimal theory, which has previously been used in the microwave regime with considerable success, can provide a basis for understanding the infrared data. We find that a number of qualitative features of the data may be understood within the current framework, but that some quantitative discrepancies remain which may provide clues to the physics missing in the minimal model.

In Section II we discuss the model and lay out the calculation of $\sigma_1(\omega, T)$. Section III contains the results and comparisons with data. Our conclusions are given in Section IV.

II. INFRARED CONDUCTIVITY

Within the BCS framework, the real part of the x -axis conductivity, here labeled as $\sigma_1(\omega)$, is given by

$$\sigma_1(\omega) = -\frac{\text{Im } \Lambda_{xx}(\omega)}{\omega}, \quad (1)$$

with

$$\text{Im } \Lambda_{xx}(\omega) = \pi e^2 \int \frac{d^2p}{(2\pi)^2} d\omega' \text{Tr} [\underline{A}(\mathbf{p}, \omega + \omega') \underline{A}(\mathbf{p}, \omega')] [f(\omega + \omega') - f(\omega')] [v_x(\mathbf{p})]^2. \quad (2)$$

Here $v_x(\mathbf{p})$ is the electron group velocity along the x -direction and $\underline{A}(\mathbf{p}, \omega)$ is the spectral weight of the Nambu propagator. That is, $\underline{A}(\mathbf{p}, \omega) = -\text{Im } \underline{G}(\mathbf{p}, \omega)/\pi$, with

$$\underline{G}(\mathbf{p}, \omega) = \frac{\tilde{\omega} \underline{\tau}^0 + \tilde{\varepsilon}_{\mathbf{p}} \underline{\tau}^3 + \tilde{\Delta}_{\mathbf{p}} \underline{\tau}^1}{\tilde{\omega}^2 - \tilde{\varepsilon}_{\mathbf{p}}^2 - \tilde{\Delta}_{\mathbf{p}}^2}, \quad (3)$$

and the $\underline{\tau}^i$ are Pauli matrices. The tilde symbols indicate inclusion of self-energy corrections: $\tilde{\omega} = \omega - \Sigma_0$, $\tilde{\varepsilon}_{\mathbf{p}} = \varepsilon_{\mathbf{p}} + \Sigma_3$, and $\tilde{\Delta}_{\mathbf{p}} = \Delta_{\mathbf{p}} + \Sigma_1$. In the calculations which follow we use $\varepsilon_{\mathbf{p}} = -2t(\cos p_x + \cos p_y) - \mu$ and $\Delta_{\mathbf{p}} = a\Delta(T)(\cos p_x - \cos p_y)$, with the parameter a chosen such that the maximum value of the gap on the Fermi surface is $\Delta(T)$. For this tight-binding band the group velocity mentioned above is given by $v_x(\mathbf{p}) = 2t \sin p_x$.

The effect of impurity scattering is included by allowing the electron self-energy to include multiple scattering from a random site potential. In this case, the self-energy is given by¹⁸

$$\Sigma_0^{\text{imp}}(\omega) = \frac{\Gamma g_0(\omega)}{c^2 - g_0^2(\omega)} ; \quad (4)$$

$$\Sigma_3^{\text{imp}}(\omega) = \frac{-\Gamma c}{c^2 - g_0^2(\omega)} .$$

Here $\Gamma = n_i/(\pi N_0)$, $c = \cot \delta_0$, and $g_0(\omega) = 1/(\pi N_0) \int d^2p \text{Tr}[\underline{G}(\mathbf{p}, \omega)]/(2\pi)^2$, where n_i is the impurity concentration, N_0 is the normal phase density of states, and δ_0 is the scattering phase shift. The self-energy correction to the gap function Σ_1 vanishes for a d -wave gap, and in the unitary limit, $c = 0$, only the Σ_0 contribution remains. In this case, the quasiparticle relaxation rate due to the impurity scattering is

$$\tau_{\text{imp}}^{-1}(\omega) = -2 \text{Im} \Sigma_0^{\text{imp}}(\omega) . \quad (5)$$

Results for τ_{imp}^{-1} versus ω for several values of Γ are shown in Fig. 2. The two smaller values of Γ were used in Ref. 16 to fit penetration depth measurements and are used again here to allow comparison with those previous results.

In order to take into account the dynamic spin-fluctuation contributions to the quasiparticle lifetime, we include, in addition to the impurity scattering, the imaginary part of the self-energy that arises from spin-fluctuation exchange

$$\begin{aligned} \text{Im} \underline{\Sigma}^{\text{sf}}(\mathbf{p}, \omega) = & \int \frac{d^2p'}{(2\pi)^2} \frac{1}{2[f(\omega) - 1]} \\ & \times \left\{ \text{Im} V(\mathbf{p} - \mathbf{p}', \omega - E_{\mathbf{p}'}) [n(\omega - E_{\mathbf{p}'}) + 1][1 - f(E_{\mathbf{p}'})] \left(\underline{\tau}^0 + \frac{\varepsilon_{\mathbf{p}'}}{E_{\mathbf{p}'}} \underline{\tau}^3 + \frac{\Delta_{\mathbf{p}'}}{E_{\mathbf{p}'}} \underline{\tau}^1 \right) \right. \\ & \left. + \text{Im} V(\mathbf{p} - \mathbf{p}', \omega + E_{\mathbf{p}'}) [n(\omega + E_{\mathbf{p}'}) + 1] f(E_{\mathbf{p}'}) \left(\underline{\tau}^0 - \frac{\varepsilon_{\mathbf{p}'}}{E_{\mathbf{p}'}} \underline{\tau}^3 - \frac{\Delta_{\mathbf{p}'}}{E_{\mathbf{p}'}} \underline{\tau}^1 \right) \right\} . \quad (6) \end{aligned}$$

Here n and f are the usual Bose and Fermi functions, and

$$V(\mathbf{q}, \omega) = \frac{3}{2} \frac{\overline{U}^2 \chi_0(\mathbf{q}, \omega)}{1 - \overline{U} \chi_0(\mathbf{q}, \omega)} , \quad (7)$$

with

$$\begin{aligned} \chi_0(\mathbf{q}, \omega) = & \int \frac{d^2p}{(2\pi)^2} \left\{ \frac{1}{2} \left[1 + \frac{\varepsilon_{\mathbf{p}+\mathbf{q}} \varepsilon_{\mathbf{p}} + \Delta_{\mathbf{p}+\mathbf{q}} \Delta_{\mathbf{p}}}{E_{\mathbf{p}+\mathbf{q}} E_{\mathbf{p}}} \right] \frac{f(E_{\mathbf{p}+\mathbf{q}}) - f(E_{\mathbf{p}})}{\omega - (E_{\mathbf{p}+\mathbf{q}} - E_{\mathbf{p}}) + i\delta} \right. \\ & \left. + \frac{1}{4} \left[1 - \frac{\varepsilon_{\mathbf{p}+\mathbf{q}} \varepsilon_{\mathbf{p}} + \Delta_{\mathbf{p}+\mathbf{q}} \Delta_{\mathbf{p}}}{E_{\mathbf{p}+\mathbf{q}} E_{\mathbf{p}}} \right] \frac{1 - f(E_{\mathbf{p}+\mathbf{q}}) - f(E_{\mathbf{p}})}{\omega_m + (E_{\mathbf{p}+\mathbf{q}} + E_{\mathbf{p}}) + i\delta} \right\} \end{aligned}$$

$$+ \frac{1}{4} \left[1 - \frac{\varepsilon_{\mathbf{p}+\mathbf{q}}\varepsilon_{\mathbf{p}} + \Delta_{\mathbf{p}+\mathbf{q}}\Delta_{\mathbf{p}}}{E_{\mathbf{p}+\mathbf{q}}E_{\mathbf{p}}} \right] \frac{f(E_{\mathbf{p}+\mathbf{q}}) + f(E_{\mathbf{p}}) - 1}{\omega - (E_{\mathbf{p}+\mathbf{q}} + E_{\mathbf{p}}) + i\delta} \Big\}, \quad (8)$$

and \bar{U} a phenomenological interaction parameter.

From Eq. (6) it follows that The inelastic spin-fluctuation induced lifetime of a quasiparticle of energy ω and momentum \mathbf{p} in a superconductor at temperature T can be written as

$$\begin{aligned} \tau_{\text{in}}^{-1}(\mathbf{p}, \omega) = \int \frac{d^2p'}{(2\pi)^2} \left[\frac{1}{1-f(\omega)} \right] & \left\{ \int_0^{\omega-|\Delta_{\mathbf{p}'|}} d\nu \text{Im} V(\mathbf{p}-\mathbf{p}', \nu) \delta(\omega-\nu-E_{\mathbf{p}'}) \right. \\ & \times \left[1 + \frac{\Delta_{\mathbf{p}}\Delta_{\mathbf{p}'} + \varepsilon_{\mathbf{p}}\varepsilon_{\mathbf{p}'}}{\omega(\omega-\nu)} \right] [n(\nu)+1][1-f(\omega-\nu)] \\ & + \int_{\omega+|\Delta_{\mathbf{p}'|}}^0 d\nu \text{Im} V(\mathbf{p}-\mathbf{p}', \nu) \delta(\nu-\omega-E_{\mathbf{p}'}) \\ & \times \left[1 - \frac{\Delta_{\mathbf{p}}\Delta_{\mathbf{p}'} + \varepsilon_{\mathbf{p}}\varepsilon_{\mathbf{p}'}}{\omega(\nu-\omega)} \right] [n(\nu)+1][f(\nu-\omega)] \\ & + \int_0^\infty d\nu \text{Im} V(\mathbf{p}-\mathbf{p}', \nu) \delta(\omega+\nu-E_{\mathbf{p}'}) \\ & \times \left. \left[1 + \frac{\Delta_{\mathbf{p}}\Delta_{\mathbf{p}'} + \varepsilon_{\mathbf{p}}\varepsilon_{\mathbf{p}'}}{\omega(\omega+\nu)} \right] n(\nu)[1-f(\omega+\nu)] \right\}. \quad (9) \end{aligned}$$

The first and third terms represent scattering processes associated with the emission and absorption of spin fluctuations, while the second term arises from the recombination of two quasiparticles to form a pair. Above T_c , $\Delta_{\mathbf{p}}$ goes to zero and Eq. (9) reduces to the usual normal state expression.

Using parameter values for the two-dimensional Hubbard model ($\langle n \rangle = 0.85$, $\bar{U} = 2$, $T_c = 0.2t$, $\Delta_0 = 3T_c$) which were previously used to model NMR relaxation time data,¹⁹ calculations of the temperature dependence of the inelastic scattering lifetime $\tau_{\text{in}}^{-1}(\mathbf{p}, \omega = T)$ were previously reported.²⁰ Here we examine the frequency dependence of $\tau_{\text{in}}^{-1}(\mathbf{p}, \omega)$. Figure 3 shows τ_{in}^{-1} versus ω for three different Fermi surface momenta.²¹ At a node, $\tau_{\text{in}}^{-1}(\mathbf{p}, \omega) \sim \omega^3$ at low energies crossing over to an approximate linear variation when $\omega \gtrsim 3\Delta(T)$. This is similar to the temperature dependence of $\tau_{\text{in}}^{-1}(\mathbf{p}, \omega = T)$ previously reported. At low energies, the usual quasiparticle-quasiparticle Coulomb scattering would vary as ω^2 . Here the extra power of ω reflects the low-energy variation of the $d_{x^2-y^2}$ -wave density of states. For energies larger than several $\Delta(T)$, $\tau_{\text{in}}^{-1}(\mathbf{p}, \omega)$ is expected to approach its normal state variation which is approximately linear for strong spin-fluctuation scattering and a nearly

nested Fermi surface. Also apparent in Fig. 3 is that for \mathbf{p} away from a gap node $\tau_{\text{in}}^{-1}(\mathbf{p}, \omega)$ varies approximately as $(\omega - \Delta_{\mathbf{p}})^3$ at low energy, crossing over to linear variation at higher energy.

The effects of both the elastic and inelastic quasiparticle lifetimes are included in the infrared conductivity calculations which follow by adding the electron self-energies due to elastic and inelastic processes

$$\underline{\Sigma}(\mathbf{p}, \omega) = \underline{\Sigma}^{\text{sf}}(\mathbf{p}, \omega) + \underline{\Sigma}^{\text{imp}}(\omega) . \quad (10)$$

This total self-energy is then used in the evaluation of Eq. (2).

To make further progress we make certain simplifying approximations for calculational simplicity. $\text{Re } \underline{\Sigma}^{\text{sf}}(\mathbf{p}, \omega)$ is not included in results presented; test calculations show that it varies slowly enough with frequency, temperature and momentum to be absorbed into an effective mass renormalization. $\text{Re } \underline{\Sigma}^{\text{imp}}(\omega)$ is retained, however, to allow for direct comparison with Refs. 12 and 15 at low frequencies. It remains to evaluate $\text{Im } \underline{\Sigma}^{\text{sf}}(\mathbf{p}, \omega)$, as given in Eq. (6). As in Ref. 20, the momentum sums in Eqs. (6) and (8) are performed by evaluating the integrands on a lattice of points covering the Brillouin zone and summing the results. (For a more detailed discussion see Ref. 22.) Since the momentum sum in Eq. (8) is nested inside that of Eq. (6), evaluation of $\text{Im } \underline{\Sigma}^{\text{sf}}(\mathbf{p}, \omega)$ is computationally rather costly. Performing this evaluation for each point of the momentum lattice sums required to evaluate Eq. (2) would be prohibitively costly since a separate momentum sum is required for each value of ω' needed to numerically evaluate the frequency integral contained therein. It is therefore a practical necessity to replace $\text{Im } \underline{\Sigma}^{\text{sf}}(\mathbf{p}, \omega)$ in Eq. (2) by an appropriate interpolation which captures the most important features of the momentum frequency and temperature dependence of $\text{Im } \underline{\Sigma}^{\text{sf}}(\mathbf{p}, \omega)$. As discussed above, the frequency and momentum dependent of $\tau_{\text{in}}^{-1}(\mathbf{p}, \omega)$ (at a temperature well below T_c) is reasonably well fit with an interpolation which varies as $(\omega - \Delta_{\mathbf{p}})^3$. One may ask whether the momentum dependence of this quantity has any influence on the infrared conductivity. Figure 4 shows two curves which represent the conductivity calculated with

$$\underline{\Sigma}^{\text{sf}}(\mathbf{p}, \omega) = -i [2\tau_{\text{in}}^*(\mathbf{p}, \omega)]^{-1} \mathcal{I}_0 \quad (11)$$

for two different choices of the interpolation function $[\tau_{\text{in}}^*(\mathbf{p}, \omega)]^{-1}$. One choice is a $(\omega - \Delta(\theta))^3$ interpolation. Another choice is to replace $\underline{\Sigma}^{\text{sf}}(\mathbf{p}, \omega)$ by its value at the gap node on the Fermi surface. This leads to a momentum-independent interpolation which varies as ω^3 for $\omega < 3\Delta_0$ and ω for $\omega > 3\Delta_0$. As may be seen, the two interpolations produce nearly identical results. For simplicity of interpretation then, a momentum-independent interpolation is used in all of the $\sigma_1(\omega)$ evaluations which follow.

Of course, in order to calculate $\sigma_1(\omega)$ at other than the lowest temperatures, we must incorporate temperature dependence in the $(\tau_{\text{in}}^*)^{-1}$ interpolation. Figure 5 shows $\tau_{\text{in}}^{-1}(\mathbf{p}^*, \omega)$, where \mathbf{p}^* is the Fermi surface wavevector at a gap node, calculated for T equal to T_c , $0.8T_c$, and $0.1T_c$. The low temperature curve shows the cubic-to-linear crossover at $3\Delta_0$ discussed above. The $T = 0.08T_c$ curve also shows a crossover at $\omega = 3\Delta(T)$, but varies more slowly than ω^3 at low temperatures. The solid curves in Fig. 5 show the interpolations used at the respective temperatures in the calculations of $\sigma_1(\omega)$.

Before giving our results, we note that vertex corrections to the conductivity have been neglected. While this is justified in the impurity-dominated regime, where s -wave impurity vertex corrections to current-current correlations functions vanish identically for singlet states, it represents a further approximation in the region where the inelastic spin fluctuations provide the dominant scattering. We ignore these corrections in what follows in order to get a qualitative picture of the conductivity in the minimal model.

III. RESULTS

Our basic results for $\sigma_1(\omega, T)$ are summarized in Figs. 6–8. Here $\sigma_1(\omega, T)$, normalized to $\sigma_0 = (ne^2/m)/(2T_c) \approx \sigma_1(0, T_c)$, is plotted versus ω for various temperatures and elastic impurity scattering parameters. A $2\Delta_0/kT_c$ ratio of 6 was chosen for these plots. Figure 6 shows $\sigma_1(\omega, T)$ for various temperatures for a unitary impurity scattering strength $\Gamma = 0.018T_c$. In the normal state at $T = T_c$, the inelastic scattering strength is dominant, leading

to an enhancement of the spectral weight over the simple Drude ω^{-2} behavior. As the temperature decreases below T_c and the $d_{x^2-y^2}$ gap opens, spectral weight is transferred into the $\omega = 0$ superfluid delta-function. A narrow “residual Drude” response due to scattering by nodal quasiparticles remains, becoming increasingly narrow and high as T/T_c decreases until the quasiparticle lifetime is limited by elastic impurity scattering. Figure 7 illustrates the effect of increasing the elastic scattering rate Γ which broadens this Drude-like response. If the impurity scattering rate in the normal state is significantly smaller than Δ_0 , this feature may be shown to persist crudely out to a frequency ω^* determined by the crossover of the elastic and the inelastic scattering rates, and corresponding roughly to the position of the low temperature conductivity minimum in Figs. 6 and 7. In the clean limit we find $\omega^* \sim (\Gamma T_c^3)^{1/4}$ if impurity scattering is resonant, and $\omega^* \sim (\Gamma_N T_c)^{1/2}$ in the weak scattering limit $c \gg 1$ (where $\Gamma_N = \Gamma/[c^2 + 1]$). At $T = 0$ the weight in the residual Drude feature is largest in the unitary limit, but increases considerably more rapidly at finite temperatures for weak scattering, as seen in Fig. 8. This may be understood in terms of the slower $T \rightarrow T^2$ crossover in the penetration depth in this case,^{23,24} reflected in the temperature dependent part of the condensate depletion. We also note that the *effective* (experimentally observable) $\omega \rightarrow 0$ conductivity in the weak scattering limit is of order $\sigma_{\text{imp}} \equiv ne^2/2m\Gamma_N$, much larger than the “universal”²⁵ resonant d-wave result $\sigma_{00} \simeq ne^2/m\pi\Delta_0$ in the clean limit.

In the resonant impurity scattering limit $c = 0$, a “shoulder” arises at $\omega = \Delta_0$ in the conductivity due to scattering of quasiparticles from the scattering resonance in the density of states at $\omega = 0$ to the peak at the gap “edge.”²⁶ Although this might in principle be used to identify the existence of strong elastic scattering, it is smeared by finite temperature effects and may thus be difficult to observe. It is seen in the $T = 0$ conductivity displayed in Fig. 6 as a kink around Δ_0 . Note there is no particular structure in the d-wave conductivity at $\omega = 2\Delta_0$.

In the limit $\tau_{\text{imp}}^{-1} \rightarrow 0$, the onset at $2\Delta_0$ in an *s*-wave superconductor is suppressed by the inability to conserve momentum and the onset appears at $4\Delta_0$, where inelastic scattering leads to a four quasiparticle final state.²⁷ For the $d_{x^2-y^2}$ case, this effect is broadened by

the gapless nature of the state; however, a broad peak at $4\Delta_0$, with Δ_0 the maximum of the $d_{x^2-y^2}$ gap, is clearly visible above the minimum conductivity at $\sim \omega^*$. The peak shifts downward and becomes larger as the quasiparticle relaxation rate becomes comparable to Δ_0 , but is near $4\Delta_0$ in the clean limit, which obtains at these frequencies if Hubbard parameters consistent with normal state data are chosen. Figure 9 shows how this broad peak shifts with $2\Delta_0/kT_c$.

To summarize, a $d_{x^2-y^2}$ BCS model in which quasiparticle damping due to impurity scattering and spin-fluctuation scattering is included gives rise to (1) a low-frequency Drude-like feature whose width and strength depend upon the impurity concentration, and (2) a midinfrared maximum at ω of order $4\Delta_0$ whose strength depends upon $2\Delta_0/kT_c$ and the strength of the inelastic scattering.

IV. CONCLUSIONS

The dashed lines in Fig. 10 show a possible fit of our model calculation of the a -axis conductivity σ_1 for the normal and superconducting states of the untwinned YBCO crystal studied in Ref. 28. The a -axis data was chosen for comparison to minimize the influence of absorption due to the YBCO chain layers. Here we have taken $\sigma_0 = 20,000 \Omega^{-1} \text{cm}^{-1}$, unitary ($c = 0$) impurity scattering with $\Gamma = 0.1 T_c$, and $2\Delta_0/kT_c = 6$. Note that the value of σ_0 is consistent with an effective mass of order 2 and a quasiparticle lifetime at T_c of order T_c^{-1} , which is what we have used.

Figure 10 demonstrates the qualitative similarity of the data to the theory, in particular the beginning of the onset of the residual Drude feature, and a conductivity peak at about 1000cm^{-1} , corresponding roughly to $4\Delta_0$. There are, however, several apparent discrepancies. Firstly, our model fails to give sufficient spectral weight at high frequencies. We believe that this represents a failure to adequately describe the normal state at these higher energies, equivalent to the discrepancies encountered when comparing the Marginal Fermi Liquid model to experiment.⁷ It may be, as recent numerical calculations suggest,^{29,30,31}

that this extra weight arises from excitations from the lower Hubbard band to the narrow quasiparticle band which forms at the upper edge of the lower Hubbard band when the system is doped away from half-filling. Such calculations also show a distinct peak at roughly $J \simeq 1000 \text{ cm}^{-1}$ in the normal state conductivity. However, a complete explanation along these lines should provide an understanding not only for the MIR peak in the normal state of $\text{YBa}_2\text{Cu}_3\text{O}_{6.6}$ and $\text{La}_{2-x}\text{Ba}_x\text{CuO}_4$, but also for its absence in $\text{YBa}_2\text{Cu}_3\text{O}_7$ and $\text{Bi}_2\text{Sr}_2\text{CaCu}_2\text{O}_8$. It has been speculated that the latter, “spin gap” materials consist in their normal state of preformed pairs which form a superconducting condensate below T_c .³² Such pair correlations might then give rise even for $T > T_c$ to the inelastic MIR peak at $4\Delta_0$ found in the current mean field theory, whereas in the former class of compounds the coherence and pairing onset temperatures coincide, so a distinct MIR peak is seen only for $T < T_c$. Finally, we note that we are not able to rule out the possibility of a separate MIR band of electronic excitations which do not participate in superconductivity.⁴

A second discrepancy arises when we try to compare values of impurity scattering rates found by fitting optical data as in Fig. 10 with those deduced from fits to the low-temperature penetration depth. In the unitary scattering limit, it was found in Ref. 16 that values of Γ of roughly $10^{-3}T_c$ were characteristic of nominally pure high quality single crystals. As seen in Fig. 10, low-frequency optical data on similar samples requires a defect scattering rate a hundred times larger within the same model. This might be taken to suggest that our treatment of the impurity t-matrix is too naive at this point. Note further that in order to obtain a consistent picture at both microwave and infrared frequencies, it is not sufficient to simply work in the Born limit,¹³ since in general increasing c at fixed normal state scattering rate decreases the weight in the residual Drude peak (Fig. 8).

However, it is important to recognize that the upturn in the $\sigma_1(\omega)$ data, obtained by a Kramers-Krönig transform of reflectance data, is extremely sensitive to the determination of the 100% reflectance point, a difficult task since resolution decreases at the lowest frequencies. Transmittance experiments,³³ which are not subject to this difficulty, appear to show a *downturn* in $\sigma_1(\omega)$ in this frequency range. This might be consistent with a true excitation

gap, but would also be consistent with a very narrow residual Drude feature below the optical resolution limit, since as $\omega \rightarrow 0$ the conductivity must rise to its DC value of roughly $2 \times 10^4 \Omega^{-1} \text{ cm}^{-1}$. We therefore believe that the apparent disagreement with experiment at low frequencies is not to be taken seriously at this time. Measurements in the far-infrared crossover region will be extremely useful to settle this point.

A clue to the phase shift due to defect scattering in these materials may be provided by a recent measurement by Homes *et al.*, in which a shoulder was observed at 300 cm^{-1} only at the lowest measurement temperature (6 K but not at 12 K) in a Ni-doped sample of optimally doped YBCO.³⁴ This small but identifiable feature is quite close to the frequency Δ_0 where we expect a shoulder due to unitary limit scattering from the Fermi level resonance to the BCS gap edge, provided $\Delta_0/T_c \simeq 3-4$.

Despite the discrepancies outlined above, the qualitative fit of this model suggests that (1) the superconducting state of YBCO is characterized by a gap with nodes and (2) the inelastic scattering at energies less than several Δ_0 is suppressed in the superconducting state. A gap with nodes can give rise to the residual Drude weight observed for $T \ll T_c$, and to an increased quasiparticle density as the impurity scattering increases due to pair-breaking processes which are present for a non-*s*-wave gap. This conclusion is supported by the irradiation experiments of Basov *et al.*¹⁴ and the Ni-doping studies of Homes *et al.*,³⁴ where the weight in the residual Drude feature clearly increases with disorder. The way in which the inelastic scattering is suppressed at frequencies less than several Δ_0 implies that the dominant dynamic interaction is electronic in nature so that its spectral weight in this region is reduced when the gap opens. The observed structure at $\sim 1000 \text{ cm}^{-1}$ is consistent with a predicted feature at $4 \Delta_0$ arising from inelastic scattering from spin fluctuations, and the smooth onset of this peak is also a natural consequence of a gapless state.

The fact that this same model provides a fit to the microwave penetration depth and a qualitative fit to the real part of the microwave conductivity provides further support for the specific picture of a $d_{x^2-y^2}$ gap with an underlying spin-fluctuation dynamic interaction.

ACKNOWLEDGMENTS

PJH is grateful for enlightening discussions with D. B. Tanner and W. O. Putikka. This work was supported by the University of Tennessee and the Division of Materials Sciences, U.S. Department of Energy, under Contract No. DE-AC05-84OR21400 with Lockheed Martin Energy Systems (SMQ), and by NSF under grant DMR92-25027 (DJS). The numerical calculations reported in this paper were performed at the San Diego Supercomputer Center.

APPENDIX: APPROXIMATE EVALUATION OF FREQUENCY-DEPENDENT CONDUCTIVITY

Here we give an approximate form of the conductivity in the current model for a $d_{x^2-y^2}$ state suitable for ready comparison with experimental data, requiring only a single numerical quadrature. The exact form of the conductivity for a flat band in the absence of vertex corrections is

$$\sigma_{\perp}(q = 0, \omega; T) = -\frac{ne^2}{m} \int d\omega' W(\omega') S_{\perp}(\omega'), \quad (\text{A1})$$

where $W(\omega'; \omega) \equiv [f(\omega' - \omega) - f(\omega')]/\omega$ and

$$S_{\perp}(\omega'; \omega) = \text{Im} \int \frac{d\phi}{2\pi} \cos^2 \phi \left[\frac{\tilde{\omega}'_+}{\tilde{\omega}_+ - \tilde{\omega}'_+} \left(\frac{1}{\xi_{0+}'} - \frac{1}{\xi_{0+}} \right) + \frac{\tilde{\omega}'_-}{\tilde{\omega}_+ - \tilde{\omega}'_-} \left(\frac{1}{\xi_{0+}} + \frac{1}{\xi_{0-}'} \right) \right]. \quad (\text{A2})$$

Here we have defined $\tilde{\omega}_{\pm} = \tilde{\omega}_{\pm}(\omega') = \omega' - \Sigma_0(\omega' \pm i0^+)$, $\xi_{0\pm} = \xi_{\pm}(\omega') = \pm \text{sgn } \omega' \sqrt{\tilde{\omega}_{\pm}^2 - \Delta_k^2}$, as well as analogous primed quantities $\tilde{\omega}'_{\pm} = \tilde{\omega}_{\pm}(\omega' - \omega)$ and $\xi'_{0\pm} = \xi_{0\pm}(\omega' - \omega)$. In general, Eq. (A2) is a complicated expression to evaluate due to the dependence of Σ_0 on $\tilde{\omega}$ and the consequent necessity of evaluating the renormalized frequencies self-consistently “in parallel” with the integral. However in a sufficiently clean system, self-consistency corrections are important only over an energy range of negligible interest for the infrared conductivity. We therefore make the replacement $\tilde{\omega}_{\pm} \rightarrow \omega' \pm i/2\tau(\omega')$, where $1/\tau(\omega)$ takes the approximate clean limit forms

$$1/\tau(\omega) \simeq \begin{cases} \min(0.6\sqrt{\Gamma\Delta_0}, \Gamma\Delta_0/|\omega|) & |\omega| < \omega^* \\ 0.08\Delta_0(|\omega|/\Delta_0)^3 & \omega^* < |\omega| < 3\Delta_0 \\ 0.7|\omega| & |\omega| > 3\Delta_0 \end{cases} \quad (\text{A3})$$

in the unitary limit and

$$1/\tau(\omega) \simeq \begin{cases} \Gamma_N|\omega|/\Delta_0 & |\omega| < \omega^* \\ 0.08\Delta_0(|\omega|/\Delta_0)^3 & \omega^* < |\omega| < 3\Delta_0 \\ 0.7|\omega| & |\omega| > 3\Delta_0 \end{cases} \quad (\text{A4})$$

in the Born limit. The crossover frequency ω^* is determined by requiring $1/\tau$ to be continuous.

The kernel S_\perp may then be simplified by retaining $1/\tau$ only in the denominators of Eq. (A2), leaving

$$S_\perp(\omega'; \omega) \simeq \frac{\omega(M' - M) - \frac{1}{2}(1/\tau - 1/\tau')(N' - N)}{2\omega^2 + \frac{1}{2}(1/\tau - 1/\tau')^2} + \frac{\omega(M - M') - \frac{1}{2}(1/\tau + 1/\tau')(N + N')}{2\omega^2 + \frac{1}{2}(1/\tau + 1/\tau')^2}. \quad (\text{A5})$$

Here $N(\omega)$ is the normalized density of states. In order to compare with the full numerical evaluation on a square lattice, we multiply the exact flat band result for a $d_{x^2-y^2}$ state over a cylindrical Fermi surface with the normalized tight-binding density of states,

$$N(\omega) \simeq \begin{cases} \frac{2|\omega|}{\pi\Delta_0} K\left(\frac{|\omega|}{\Delta_0}\right) \frac{N_t(\omega)}{N_t(0)} & |\omega| < \Delta_0 \\ \frac{2}{\pi} K\left(\frac{\Delta_0}{|\omega|}\right) \frac{N_t(\omega)}{N_t(0)} & |\omega| > \Delta_0 \end{cases}, \quad (\text{A6})$$

where K is the complete elliptic integral of the first kind. Similarly, $M(\omega)$ is approximated by

$$M(\omega) \simeq \begin{cases} \frac{2\omega}{\pi\Delta_0} K\left(\frac{\sqrt{\Delta_0^2 - \omega^2}}{\Delta_0}\right) \frac{N_t(\omega)}{N_t(0)} & |\omega| < \Delta_0 \\ 0 & |\omega| > \Delta_0 \end{cases}. \quad (\text{A7})$$

The tight-binding density of states $N_t(\omega)$ is given by

$$N_t(\omega) = \frac{1}{2\pi^2 t} K\left(\sqrt{1 - \left(\frac{\omega + \mu}{4t}\right)^2}\right). \quad (\text{A8})$$

In Eq. (A5), unprimed quantities M , N , and $1/\tau$ are evaluated at ω' , whereas primed quantities are evaluated at $\omega' - \omega$. Substitution into Eq. (A1) yields an approximation which

compares well to the full numerical evaluation, with an error of only a few percent, as shown in Fig. 11.

Note that the correct high-frequency limit of the conductivity in the case of inelastic scattering is *not* given by the usual Drude expression with $1/\tau = 1/\tau(\omega)$. For example, in the case of a flat band and $1/\tau(\omega) = b\omega$, the correct high-frequency limit obtained from Eqs. (A1) and (A2) is

$$\sigma_1 \rightarrow \left(\frac{ne^2}{m} \right) \frac{b/(2\omega)}{1 + b^2/4}, \quad (\text{A9})$$

not $\sigma_1 \rightarrow (ne^2/m)[(b/\omega)/(1 + b^2)]$.

REFERENCES

- ¹ S. B. Nam, *Phys. Rev.* **156**, 470 (1967).
- ² G. Brandi and A. J. Sievers, *Phys. Rev. B* **5**, 3350 (1972).
- ³ N. E. Bickers, D. J. Scalapino, R. T. Collins, and Z. Schlesinger, *Phys. Rev. B* **42**, 67 (1990).
- ⁴ D. B. Tanner *et al.*, *J. Phys. Chem. Solids* **53**, 1611 (1992).
- ⁵ D. N. Basov *et al.*, *Phys. Rev. Lett.* **74**, 598 (1995).
- ⁶ C. M. Varma *et al.*, *Phys. Rev. Lett.* **63**, 1996 (1989); P. B. Littlewood and C. M. Varma, *J. Appl. Phys.* **69**, 4979 (1991).
- ⁷ E. J. Nicol, T. Timusk, D. B. Tanner, and J. P. Carbotte, *Phys. Rev. B* **43**, 473 (1991).
- ⁸ T. Timusk and D. B. Tanner, in *Physical Properties of High Temperature Superconductors*, edited by D. M. Ginsberg (World Scientific, Singapore), Vol. I, p. 339 (1989); Vol. III, p. 363 (1992).
- ⁹ K. Kamaras *et al.*, *Phys. Rev. Lett.* **59**, 919 (1987).
- ¹⁰ Z. Schlesinger, R. T. Collins, D. L. Kaiser, and F. Holtzberg, *Phys. Rev. Lett.* **59**, 1958 (1987); Z. Schlesinger *et al.*, *ibid.* **65**, 801, 1990.
- ¹¹ Z. X. Shen *et al.*, *Phys. Rev. Lett.* **70**, 1553 (1993); W. N. Hardy *et al.*, *ibid.* **71**, 2134, 1993; D. A. Wollman *et al.*, *ibid.* **71**, 2134, 1993; C. C. Tsuei *et al.*, *ibid.* **73**, 593, 1993; D. A. Wollman, D. J. Van Harlingen, J. Giapintzakis, and D. M. Ginsberg, *ibid.* **74**, 797, 1995.
- ¹² W. O. Putikka and P. J. Hirschfeld, *Physica B* **194–196**, 1517 (1994).
- ¹³ J. P. Carbotte, C. Jiang, D. N. Basov, and T. Timusk, *Phys. Rev. B* **51**, 11798 (1995).
- ¹⁴ D. N. Basov *et al.*, *Phys. Rev. B* **49**, 12165 (1994).

- ¹⁵ M. J. Graf, M. Palumbo, D. Rainer, and J. A. Sauls, *Phys. Rev. B* (to be published).
- ¹⁶ P. J. Hirschfeld, W. O. Putikka, and D. J. Scalapino, *Phys. Rev. Lett.* **71**, 3705 (1993); *Phys. Rev. B* **50**, 10250 (1994).
- ¹⁷ D. A. Bonn *et al.*, *Phys. Rev. B* **47**, 11314 (1993); *J. Phys. Chem. Solids* **54**, 1297 (1993).
- ¹⁸ P. J. Hirschfeld, P. Wölfle, and D. Einzel, *Phys. Rev. B* **37**, 83 (1988); K. Scharnberg *et al.*, *Solid State Commun.* **60**, 535 (1986); H. Monien, K. Scharnberg, and D. Walker, *ibid.* **61**, 581 (1987).
- ¹⁹ N. Bulut and D. J. Scalapino, *Phys. Rev. Lett.* **68**, 706 (1992).
- ²⁰ S. M. Quinlan, D. J. Scalapino, and N. Bulut, *Phys. Rev. B* **49**, 1470 (1994).
- ²¹ Note that $\tau_{\text{in}}^{-1}(\mathbf{p}, \omega)$ is a slowly varying function of $\varepsilon_{\mathbf{p}}$ and its dominant variation is with angular position on the Fermi surface.
- ²² S. M. Quinlan, Ph.D. thesis, University of California, Santa Barbara, 1994.
- ²³ P. Arberg *et al.*, *Solid State Commun.* **86**, 671 (1993).
- ²⁴ P.J. Hirschfeld and N. Goldenfeld, *Phys. Rev. B* **48**, 4219 (1993).
- ²⁵ P. A. Lee, *Phys. Rev. Lett.* **71**, 1887 (1993).
- ²⁶ P. J. Hirschfeld *et al.*, *Phys. Rev. B* **40**, 6695 (1989).
- ²⁷ J. Orenstein *et al.*, in *Electronic Properties of High- T_c Superconductors*, edited by H. Kuzmany (Springer-Verlag, Berlin, 1990).
- ²⁸ T. A. Friedmann *et al.*, *Phys. Rev. B* **42**, 6217 (1990).
- ²⁹ E. Dagotto, *Rev. Mod. Phys.* **66**, 763 (1994).
- ³⁰ M. Jarrell, J. K. Freericks, and T. Pruschke, *Phys. Rev. B* **51**, 11704 (1995).
- ³¹ N. Bulut, D. J. Scalapino, and S. R. White, *Phys. Rev. Lett.* **72**, 705 (1994).

³² M. Randeria, N. Trivedi, A. Moreo, and R. T. Scalettar, *Phys. Rev. Lett.* **69**, 2001 (1992).

³³ D. B. Romero *et al.*, *Phys. Rev. Lett.* **68**, 1590 (1992).

³⁴ C. C. Homes, Q. Song, and B. P. Clayman (unpublished).

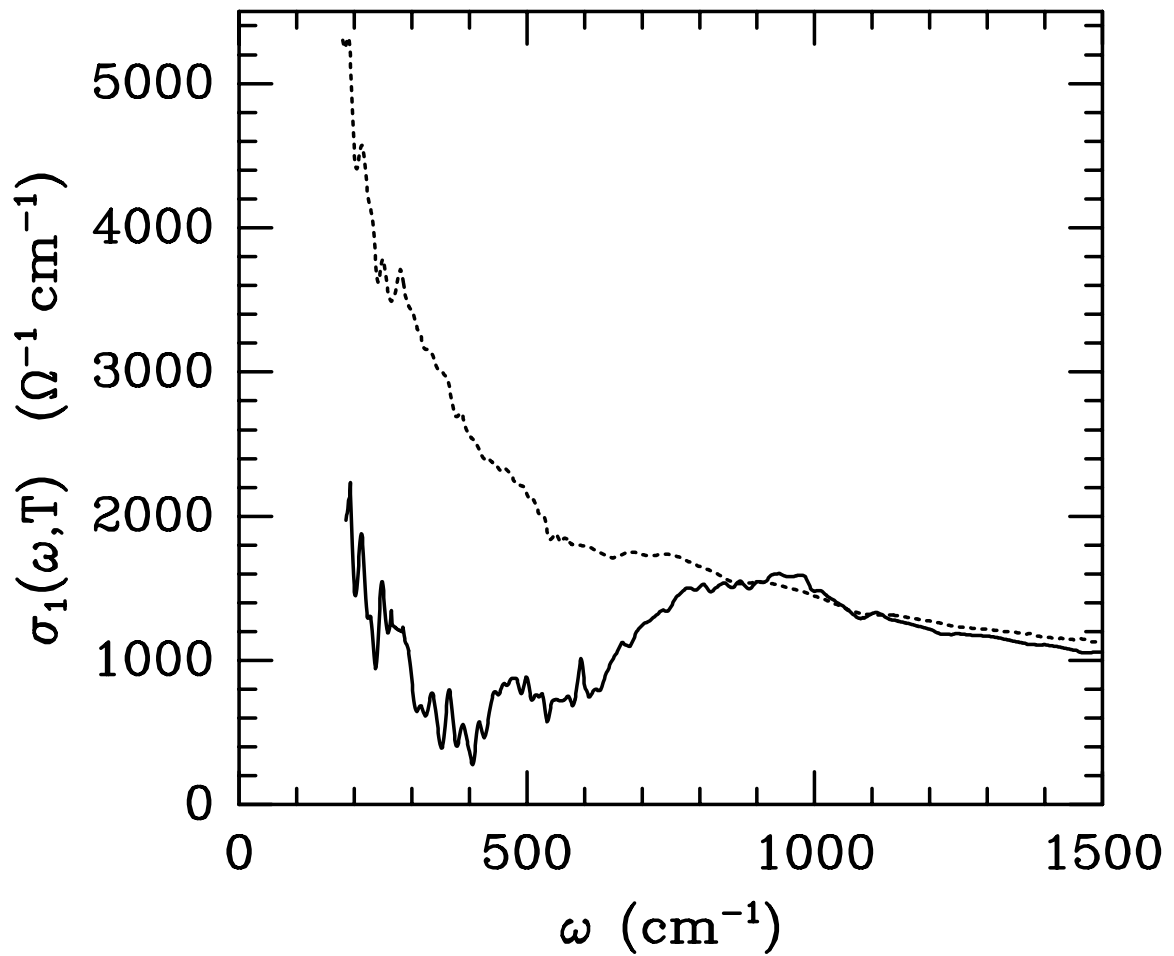


FIG. 1. Experimental results for the real part of the a -axis conductivity in the normal, $T = 100\text{K}$ (dotted line), and superconducting, $T = 20\text{K}$ (solid line), states of an untwinned YBCO crystal.⁵

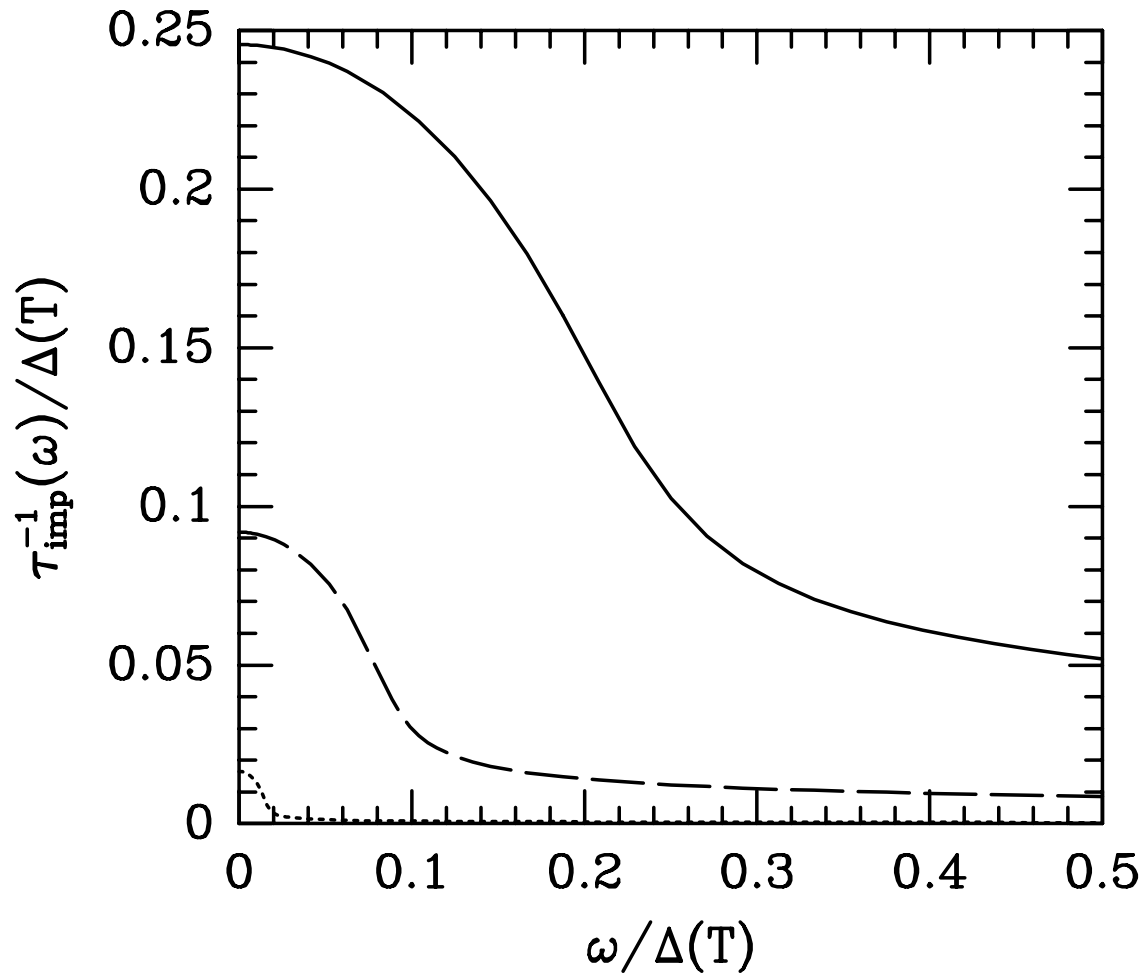


FIG. 2. Quasiparticle relaxation rate τ_{imp}^{-1} due to impurity scattering in the unitary limit, $c = 0$. Results are shown for $\Gamma = 0.0008T_c$ (dotted line), $\Gamma = 0.018T_c$ (dashed line), $\Gamma = 0.1T_c$ (solid line).

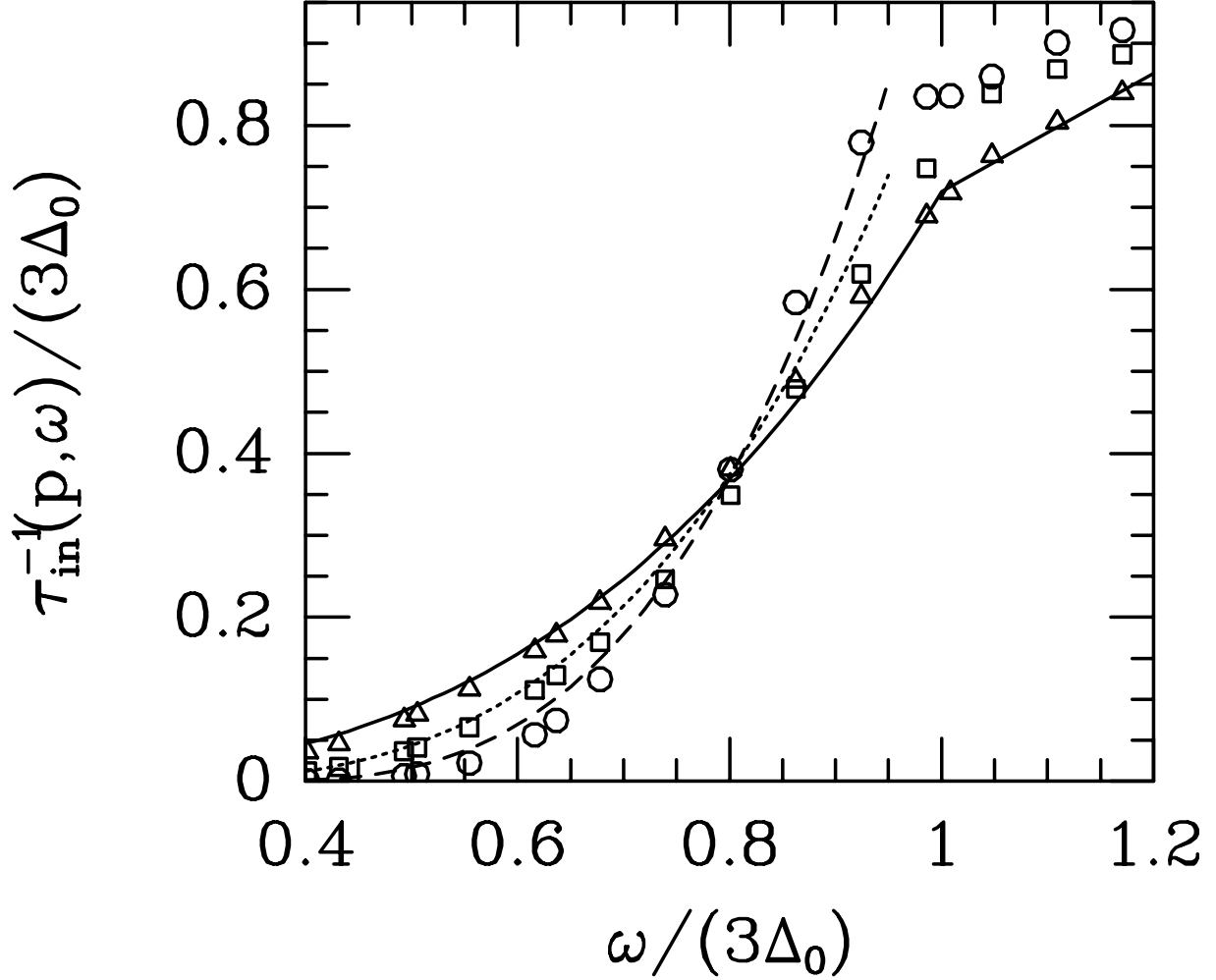


FIG. 3. Quasiparticle relaxation rate $\tau_{\text{in}}^{-1}(\mathbf{p}, \omega)$ due to spin-fluctuation scattering. Results are shown as a function of frequency for $T = 0.1T_c$. The different symbols indicate values calculated for \mathbf{p} at three different points along the Fermi surface: a gap node (triangles), a gap antinode (circles), and a point halfway between the node and the antinode (squares). The solid line shows an interpolation which varies as ω for $\omega > 3\Delta_0$ and as ω^3 for $\omega < 3\Delta_0$. The dashed lines vary as $[\omega - \Delta_{\mathbf{p}}]^3$ with \mathbf{p} , as above, at an antinode (long dashes) and an intermediate point (short dashes).

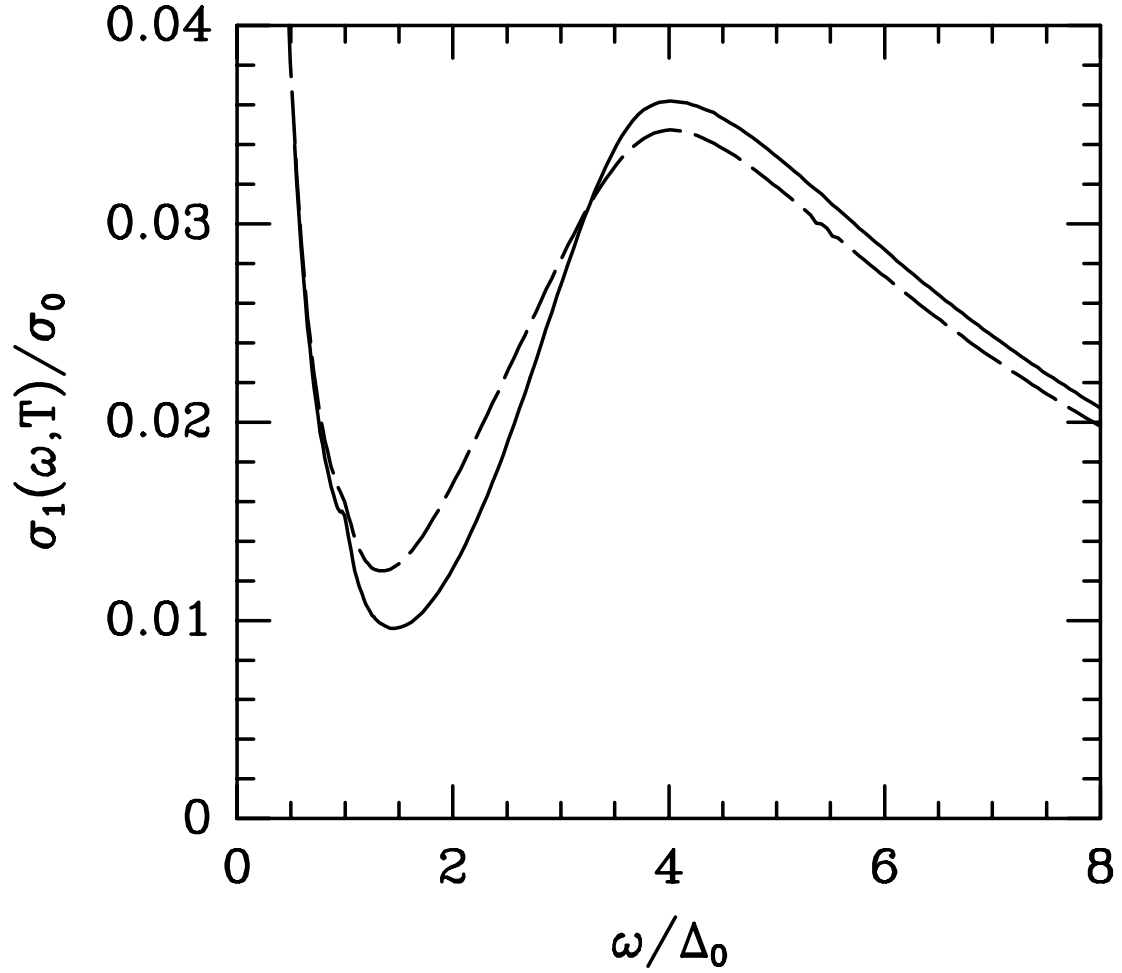


FIG. 4. Real part of the in-plane conductivity in the superconducting state for $T = 0$ and $\Gamma = 0.018T_c$. The two curves show results for two different choices for the self energy due to spin-fluctuation scattering. The solid curve incorporates the full momentum dependence reflected in Fig. 3. The dashed curve replaces $\Sigma^{\text{sf}}(\mathbf{p}, \omega)$ everywhere by its value at the gap node on the Fermi surface.

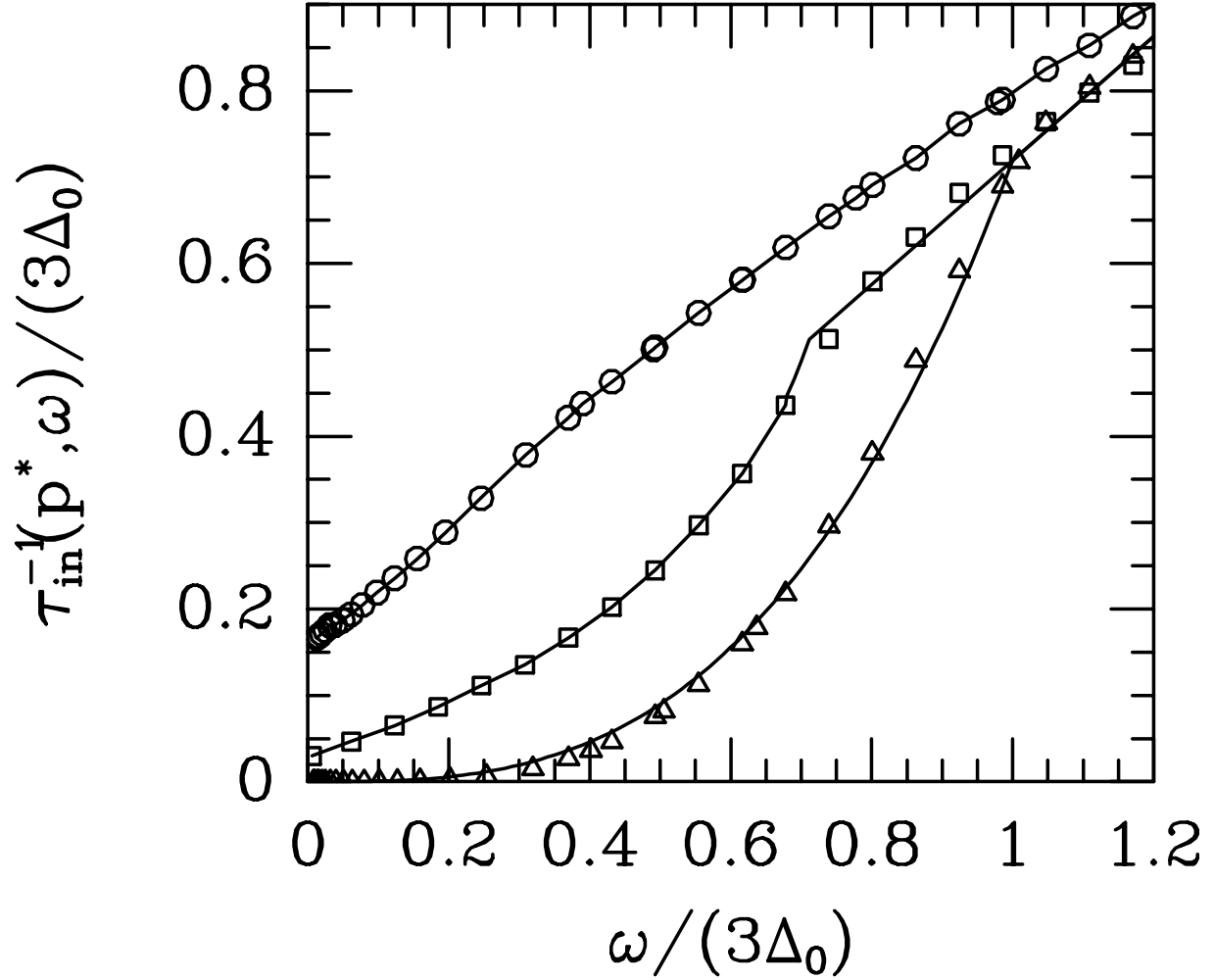


FIG. 5. Quasiparticle relaxation rate τ_{in}^{-1} due to spin-fluctuation scattering. Results are shown as a function of frequency for $T = T_c$ (circles), $T = 0.8T_c$ (squares), and $T = 0.1T_c$ (triangles). The solid lines show interpolations used at each temperature for the evaluation of $\sigma_1(\omega)$.

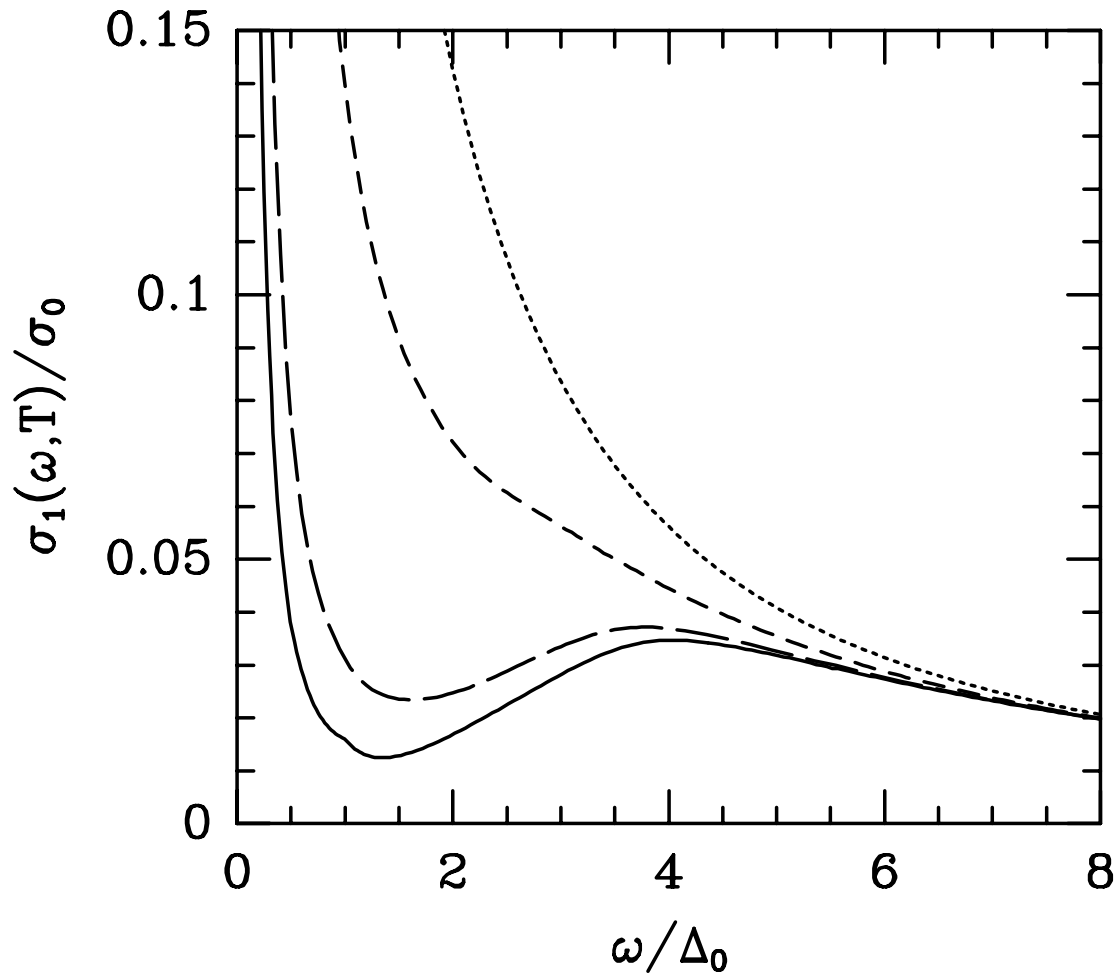


FIG. 6. Real part of the in-plane conductivity for $\Gamma = 0.018T_c$ at several different temperatures. Results are shown for $T = T_c$ (dotted line), $T = 0.8T_c$ (short dashes), $T = 0.5T_c$ (long dashes), and $T = 0$ (solid line).

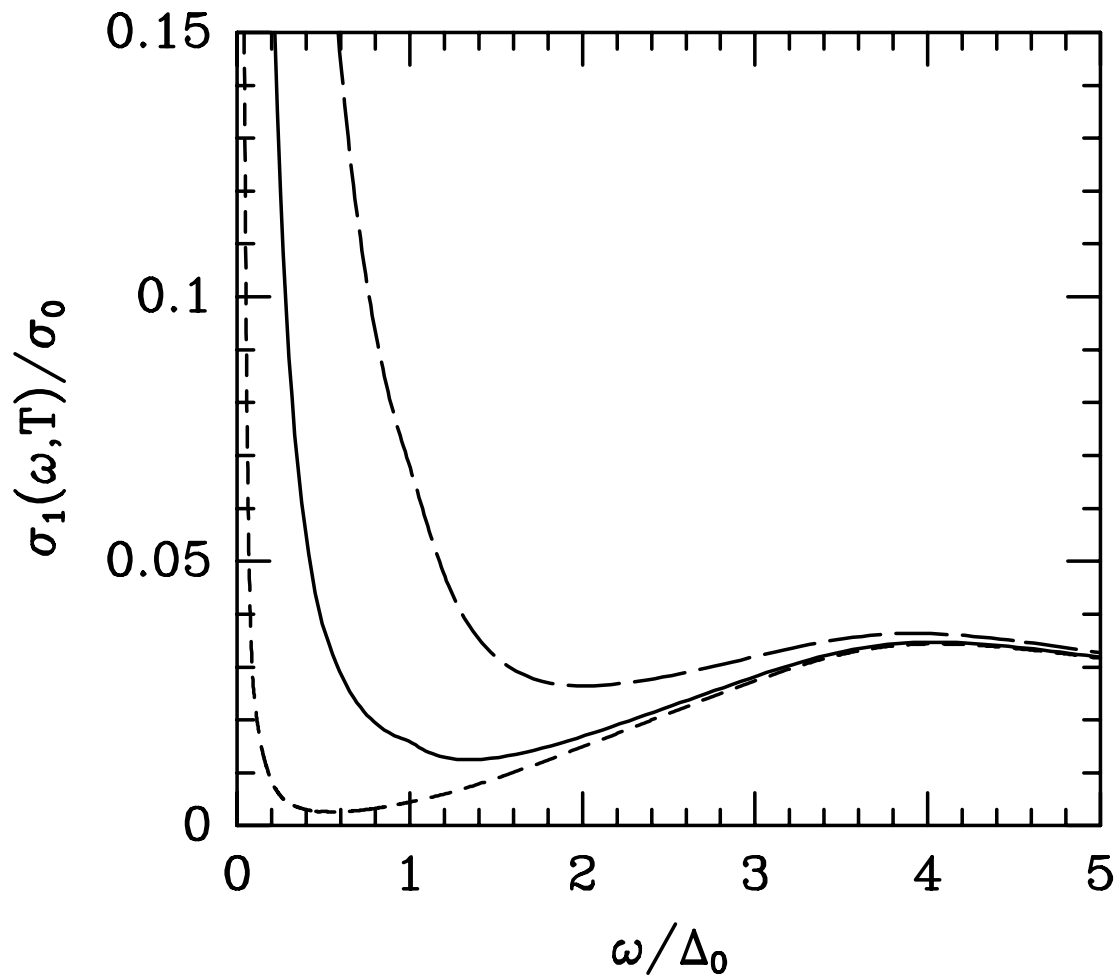


FIG. 7. Real part of the in-plane conductivity in the superconducting state ($T = 0$). Results are shown for $\Gamma = 0.0008T_c$ (short dashes), $\Gamma = 0.018T_c$ (solid line), and $\Gamma = 0.1T_c$ (long dashes)

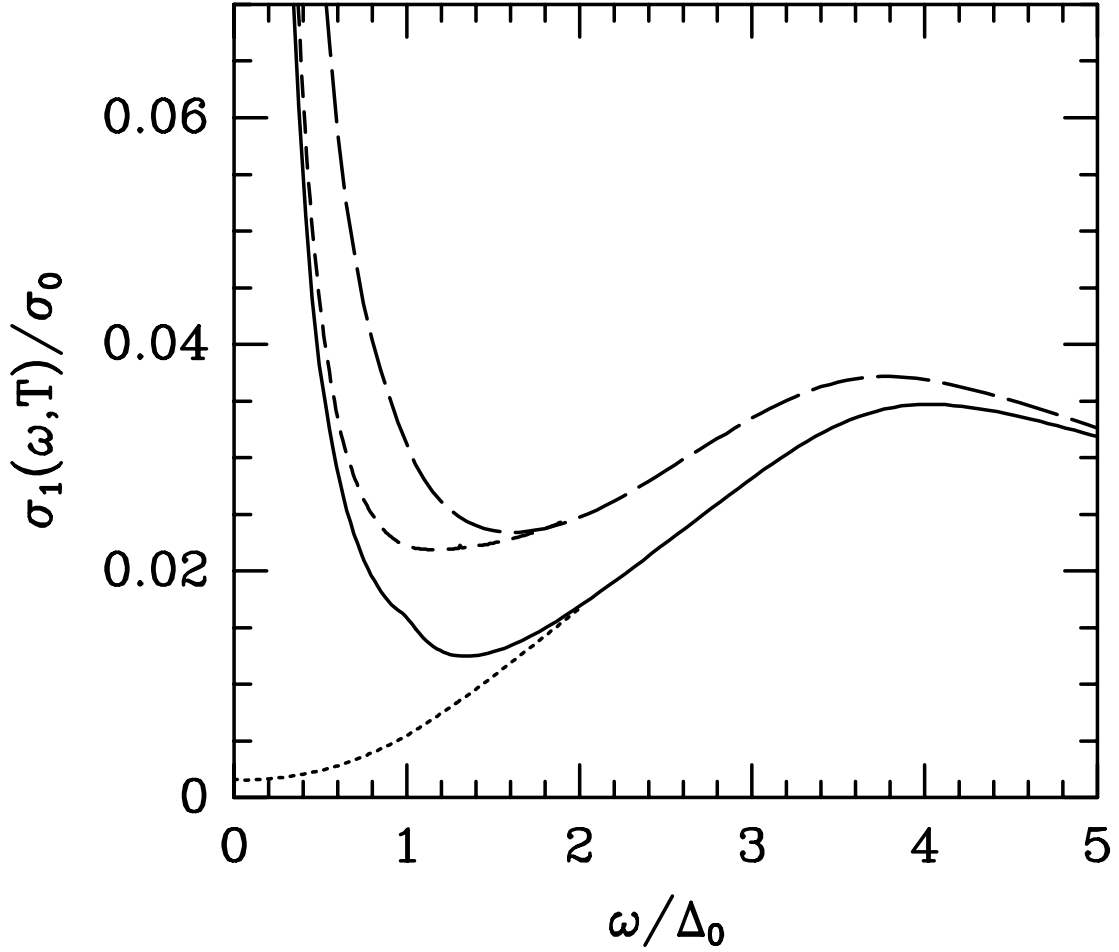


FIG. 8. Real part of the in-plane conductivity in the superconducting state for impurity scattering in the Born, $c \gg 1$ (dashed line), and unitary, $c = 0$ (solid line), limits. Curves are shown for $T = 0$ (dotted line is the Born limit, solid line is the unitary limit) and for $T = 0.5T_c$ (short dashes show the Born limit, long dashes show the unitary limit) All curves are calculated using $\Gamma/(c^2 + 1) = 0.018T_c$.

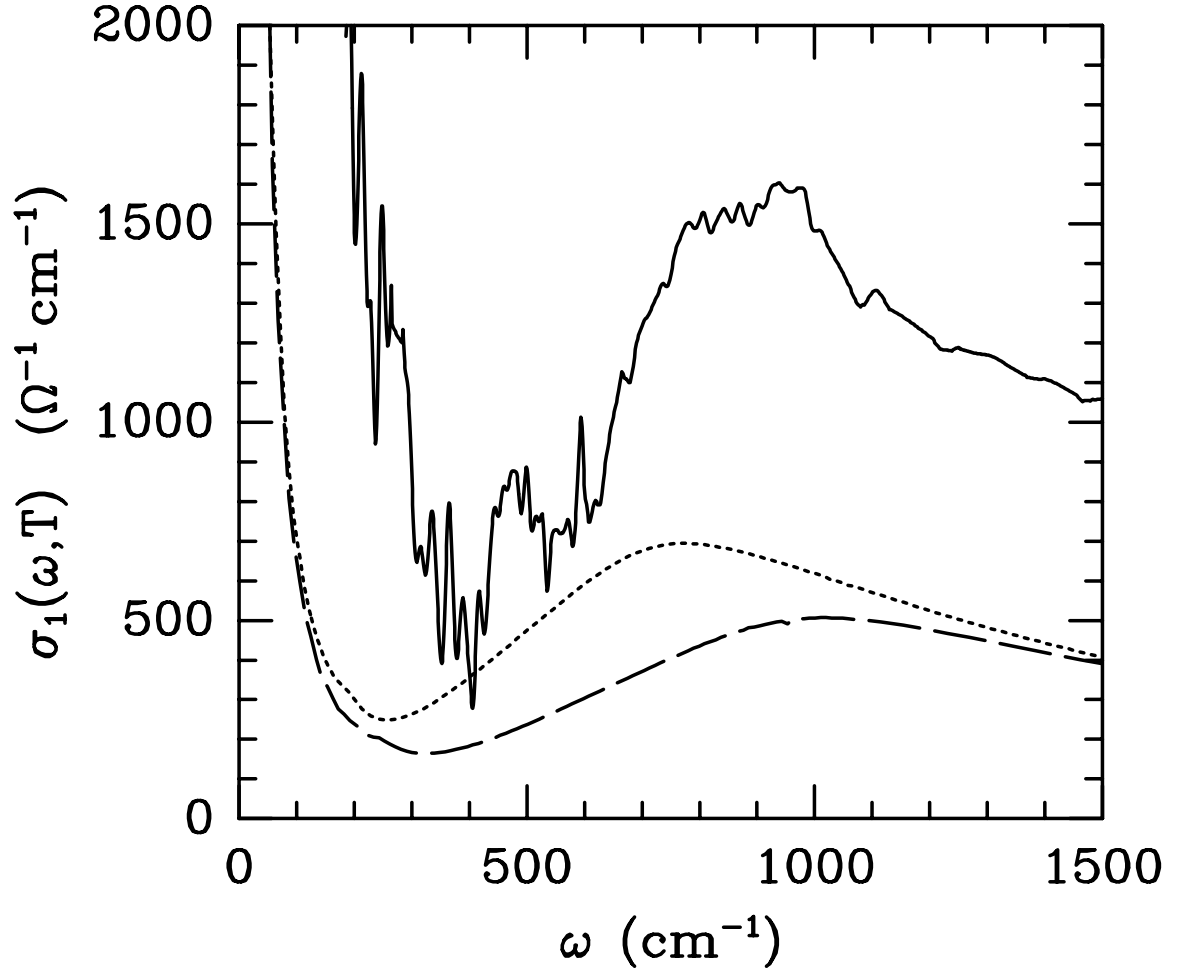


FIG. 9. Real part of the in-plane conductivity in the superconducting state calculated for two different choices for the superconducting gap ratio. Results are shown for $\Delta(0) = 3T_c$ (dotted line) and $\Delta(0) = 4T_c$ (dashed line). The solid line shows the experimental result for a -axis conductivity in the superconducting state, $T = 20$ K, of an untwinned YBCO crystal.⁵

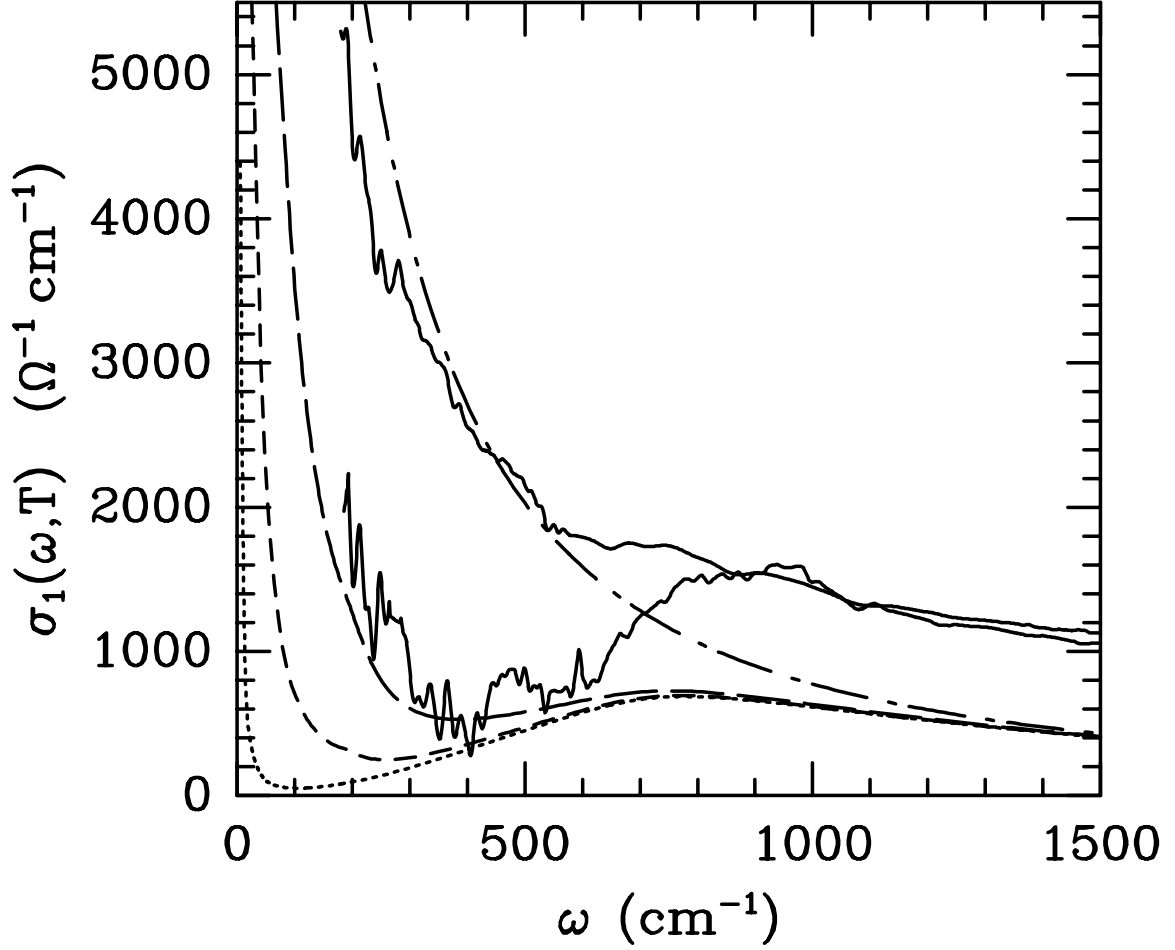


FIG. 10. Real part of the in-plane conductivity calculated for the normal, $T = T_c$ and $\Gamma = 0.018T_c$ (dot-dashed line), and superconducting, $T = 0.1T_c$, states compared to experimental results. Calculated superconducting state results are shown for $\Gamma = 0.0008T_c$ (dotted line), $\Gamma = 0.018T_c$ (short dashes), and $\Gamma = 0.1T_c$ (long dashes). The solid lines show experimental results for a -axis conductivity in the normal, $T = 100 \text{ K}$, and superconducting, $T = 20 \text{ K}$, states of an untwinned YBCO crystal.⁵

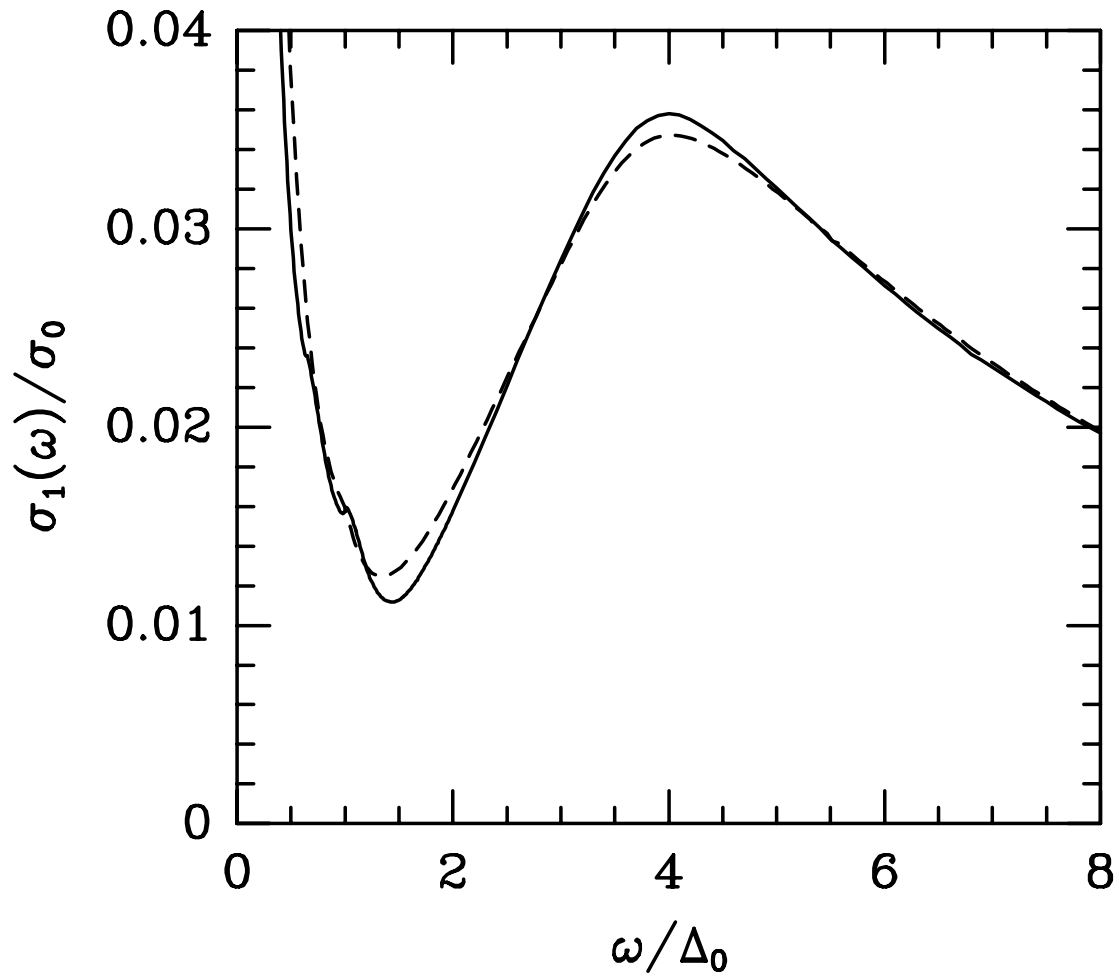


FIG. 11. A comparison of the results for the real part of the in-plane conductivity in the superconducting state (for $T = 0$ and $\Gamma = 0.018T_c$) obtained from evaluation of Eq. (1) (dashed line) and Eq. (A1) (solid line).